DERIVATION OF CYCLIC *p-y* CURVES FROM INSTRUMENTED DYNAMIC LATERAL LOAD TESTS

S.-S. Lin [*] **C.-H. Lai** [**]

Department of Harbor and River Engineering
National Taiwan Ocean University
Keelung, Taiwan 20224, R.O.C.

C.-H. Chen [**] **T.-S. Ueng** [***]

Department of Civil Engineering
National Taiwan University
Taipei, Taiwan 10617, R.O.C.

ABSTRACT

In this paper, an efficient method is proposed to derive cyclic *p-y* curves from either push-over or shaking table test results. The Fourier series function, satisfying the boundary conditions of a pile, is used to represent deflection behavior of the pile-soil system at each instant of time during loading interval. In order to obtain soil reaction along the pile shaft, convergence of the series after differentiation is guaranteed by applying the Cesaro sum technique. Results of four push-over tests and two other shaking table test results, conducted at the National Center for Research on Earthquake Engineering in Taiwan, are then used to verify the feasibility of the proposed method.

Keywords : Pile, Cyclic *p-y* curve, Cesaro sum technique, Push-over test, Shaking table test.

1. INTRODUCTION

Studies on pile foundation performance resulting from lateral cyclic or dynamic loading are often analyzed using the beam on Winkler foundation model, through nonlinear springs in the form of *p-y* curves. In this method p represents soil resistance to a pile and *y* is the corresponding displacement of the pile relative to the free field.

To derive *p-y* curves, strain gages are often installed along the length of pile shaft to develop the bending moment versus depth relationship [1-3]. Generally speaking, this involves three steps of *p-y* curve derivation [4]: (a) deriving the deflection versus depth profiles using double integration technique on the curvature versus depth profiles of a pile from stain data; (b) determining the moment versus depth profiles based on the curvature versus depth profile; and (c) deriving *p*, soil resistance per unit length of a pile, using the double differentiation technique on the moment versus depth profiles. Since the strain gages are installed at certain discrete locations along the pile, a curve fitting technique is necessary to obtained the soil resistance and deflections along the pile shaft at each instant of time. However, the derived soil resistance often becomes inaccurate due to amplification of double differentiation of discrete data points. Additional numerical technique is required to minimize the errors resulted from double differentiation. As reviewed by Yang and Liang [4], many techniques have been used to minimize this numerical error resulted from double differentiation, such as high order global polynomial curve fitting [5], Piecewise polynomial curve fitting [6], cubic spline [7,8], weighted residuals method [9], and smoothed weighted residuals method [4]. The B-splines fixed by a weighted least-squares algorithm was used by Sousa Coutinho [10] to fit the curves representing strains along the tested drilled shaft. Three separate polynomials were used to fit the bending moment profile by Dyson and Randolph [11]. A load transfer function was also fitted by means of an optimization program to reduce the potential errors involved in double differentiating the moment profile. Boundary conditions of the pile are neglected in the fitting curve among some of the available methods.

Inclinometer is another alternative for providing a measure of slope or tilt along depth of pile. The slope distribution can be easily converted to lateral displacement, however, it is prone to reduction errors due to three times differentiation for obtained soil resistance.

[*] Professor, corresponding author [**] Graduate student [***] Professor

Again, numerical techniques, such as piecewise quadratic curve fitting, piecewise cubic curve fitting, piecewise fitting of circular arcs, and global higher-order polynomial curve fitting methods have been reviewed and compared by Ooi and Ramsey [12]. Brown *et al*. [13] utilized a least-squares regression technique that converges to a solution for analytical *p-y* curves which produces minimum error between the predicted and measured deflection versus depth profile over a range of loading. A method that requires iterating a single parameter and modulus of lateral soil reaction was used by Pinto *et al*. [14]. This method assumes that the initial slope of the *p-y* curve increases linearly with depth and hence can only be used for uniform sand condition. A new method using Cesaro sum technique, which has been successfully used for single pile and pile group *p-y* curve derivation, has been adopted by Lin and Liao [2] and Lin *et al*. [3].

The purpose of this paper focuses on using the Cesaro sum technique [15] to derive the *p-y* curves from cyclic lateral pile load test results. The pile-soil interaction response is idealized as a beam on Winkler spring medium. Fourier series functions are used to represent the deflection function of the pile-soil system at each instant of time during the dynamic effect. Convergence of the series after differentiation is guaranteed by applying the Cesaro sum technique. Since the measured deflections at selected locations along shaft are used to calibrate the assumed deflection function at each instant of time, possible nonlinear soil-structure interaction is implicitly included in the analysis. Consequently, possible decay of the soil resistance versus deflection relationship due to cyclic loading is taken into account in the derived *p-y* curves. Part of the experimental results from four push-over tests and two other shaking table tests conduced by Ueng [16] at National Center for Research on Earthquake Engineering (NCREE) in Taiwan are then used to demonstrate application of the proposed methodology. Detail description of the shaking table and push-over test results is beyond the scope of this paper, readers can refer to Ueng [16] for further reading on the subject matter.

2. THEORY

In the following sections, the governing equation of the pile-soil system subjected to dynamic loading is derived first. Measured strain gage data are utilized to determine the coefficients of the derived curvature function. Subsequently, how the *p-y* curves are derived from the established curvature function is detailed at the end of the section.

2.1 Governing Equation

The total energy for a pile embedded in a soil medium is given as

$$\prod = U + V \tag{1}$$

where U = strain energy stored in the pile; and V = potential energy of soil-pile system caused by external loads.

The strain energy of the pile can be expressed as

$$U = \frac{1}{2}\int_0^L EI\left(\frac{\partial^2 y(z,\ t)}{\partial z^2}\right)^2 dz \tag{2}$$

where E = elastic modulus of the pile; I = moment of inertia of the pile; $y(z,\ t)$ = lateral deflection of the pile at depth z at time t; and L = pile length.

Assuming the soil response is idealized as one dimensional, the potential energy of the soil-pile system caused by external loading applied instantaneously can be expressed as

$$V = \frac{1}{2}\int_0^L p(z,\ t)y(z,\ t)\ dz - \frac{1}{2}\int_0^L H(z,\ t)y(z,\ t)\ dz \tag{3}$$

where $p(z,\ t)$ = soil reaction at depth z at time t; and $H(z,\ t)$ = dynamic lateral forces.

For soil reactions along shaft

$$p(z) = k_s\ y(z,\ t)\ ,\quad 0 \le z \le h \tag{4}$$

$$p(z) = 0\ ,\quad h \le z \le L \tag{5}$$

where k_s = coefficient of subgrade horizontal reaction; h = embedded length of the pile.

Substituting (2) and (3) into (1), the total potential energy of the soil-pile system can be presented as

$$\prod = \frac{1}{2}\int_0^L EI\left(\frac{\partial^2\ y(z,\ t)}{\partial z^2}\right)^2 dz + \frac{1}{2}\int_0^L p(z,\ t)\ y(z,\ t)\ dz - \frac{1}{2}\int_0^L H(z,\ t)\ y(z,\ t)\ dz \tag{6}$$

By applying the calculus of variations to (6), the following Euler-Lagrangian governing equations for the pile-soil system can be obtained

$$EIy(z,\ t)^{IV} + p(z,\ t) - H(z,\ t) = 0 \tag{7}$$

Subsequently, by applying the Rayleigh-Ritz method, the general form of the deflection that satisfies (7) can be determined by the following Fourier series as

$$y(z,\ t) = \sum_{n=1}^{k} B_n(t)\cdot\left(1 - \cos\frac{2n-1}{2L}\pi z\right) \tag{8}$$

where $B_n(t)$ = coefficients, which can be determined by substituting (8) into (6) and minimizing the function ($\partial\Pi/\partial B_n = 0$). Hence, we have

$$\prod = U + V$$

$$= \sum_{n=1}^{k} \left[\frac{EI}{8} \frac{2n-1}{2L} \pi \left((2n-1) + Sin(2n-1)\pi \right) B_n^2(t) + \frac{EI}{8} \left(\frac{2n-1}{2L} \right)^3 \pi^3 \left(\frac{(2n-1)h}{L} \pi - 4Sin \frac{(2n-1)h}{2L} \pi + Sin \frac{(2n-1)h}{L} \pi \right) B_n^2(t) - \frac{L}{(2n-1)\pi} H(z,\ t) \left((L-h) \frac{2n-1}{2L} \pi + Sin \frac{(2n-1)h}{2L} \pi - Sin \frac{(2n-1)\pi}{2} \right) B_n(t) \right] \tag{9}$$

Minimizing the function, $\frac{\partial \prod}{\partial B_n} = 0$,

$$\frac{EI}{4} \frac{2n-1}{2L} \pi \left((2n-1) + Sin(2n-1)\pi \right) B_n(t) + \frac{EI}{4} \left(\frac{2n-1}{2L} \right)^3 \pi^3 \left(\frac{(2n-1)h}{L} \pi - 4Sin \frac{(2n-1)h}{2L} \pi + Sin \frac{(2n-1)h}{L} \pi \right) B_n(t) - \frac{L}{(2n-1)\pi} H(z,\ t) \left((L-h) \frac{2n-1}{2L} \pi + Sin \frac{(2n-1)h}{2L} \pi - Sin \frac{(2n-1)\pi}{2} \right) = 0 \tag{10}$$

coefficients $B_n(t)$ can be obtained as

$$B_n(t) = \frac{-\left(2H(z,\ t) \left((L-h)\overline{N}\pi + Sin\overline{N}h\pi - Sin\overline{N}\pi \right) \right)}{EI\overline{N}^2\pi^2 \left((2n-1)\pi - 2h\overline{N}^3\pi^3 + 4\overline{N}^2\pi^2 Sin\overline{N}h\pi - \overline{N}^2\pi^2 Sin2h\overline{N}\pi + Sin2L\overline{N}\pi \right)} \tag{11}$$

where $\overline{N} = \frac{2n-1}{2L}$ for the pile with boundary conditions of free head and fixed end.

2.2 Regularization by Cesàro Sum Technique

Since the deflection functions of the pile-soil system given in Eq. (8) are Fourier series functions, these functions will cause ill-posed conditions after differentiation. The Cesaro sum technique is used to guarantee the convergence of these Fourier series functions.

The general Cesàro sum is defined as [15]

$$S_k = (C,\ r) \left\{ \sum_{n=0}^{k} a_n \right\} \equiv \frac{C_{r-1}^{k+r-1} s_0 + C_{r-1}^{k+r-2} s_1 + \cdots + C_{r-1}^{r} s_{k-1} + C_{r-1}^{r-1} s_k}{C_r^{k+r}} \tag{12}$$

where $(C,\ r) = C_r^k = \frac{k!}{\left(r!(k-r)! \right)}$ and the partial sum is $S_k = \sum_{n=0}^{k} a_n(z,\ t)$, where $a_n(z,\ t) = B_n(t) \cdot (1 - \cos \overline{N}\pi z)$.

For computational convenience, a_k terms are replaced by s_k, hence the Cesàro sum can be expressed as

$$S_k = (C,\ 1) \left\{ \sum_{n=0}^{k} a_n \right\} \equiv \frac{s_0 + s_1 + \cdots + s_{k-1} + s_k}{k+1} \tag{13}$$

$$(C,\ 1) \left\{ \sum_{n=0}^{k} a_n \right\} \equiv \sum_{n=0}^{k} \frac{k-n+1}{k+1}\ a_n \tag{14}$$

Similarly, when r = 2, 3, 4, and 5, the corresponding Cesaro sums of (C, 2), (C, 3), (C, 4), and (C, 5) are

$$(C,\ 2) \left\{ \sum_{n=0}^{k} a_n \right\} \equiv \sum_{n=0}^{k} \frac{(k-n+1)\cdot(k-n+2)}{(k+1)\cdot(k+2)}\ a_n \tag{15}$$

$$(C,\ 3) \left\{ \sum_{n=0}^{k} a_n \right\} \equiv \sum_{n=0}^{k} \frac{(k-n+1)\cdot(k-n+2)\cdot(k-n+3)}{(k+1)\cdot(k+2)\cdot(k+3)}\ a_n \tag{16}$$

$$(C,\ 4) \left\{ \sum_{n=0}^{k} a_n \right\} \equiv \sum_{n=0}^{k} \frac{(k-n+1)\cdot(k-n+2)\cdot(k-n+3)\cdot(k-n+4)}{(k+1)\cdot(k+2)\cdot(k+3)\cdot(k+4)}\ a_n \tag{17}$$

$$(C,\ 5) \left\{ \sum_{n=0}^{k} a_n \right\} \equiv \sum_{n=0}^{k} \frac{(k-n+1)\cdot(k-n+2)\cdot(k-n+3)\cdot(k-n+4)\cdot(k-n+5)}{(k+1)\cdot(k+2)\cdot(k+3)\cdot(k+4)\cdot(k+5)}\ a_n \tag{18}$$

Based on this regularization procedure, the series representations for displacement $y(z, t)$, slope $S(z, t)$, moment $M(z, t)$, shear force $V(z, t)$, and soil reaction $p(z, t)$ are expressed in the sense of the Cesaro sum as

$$y(z,\ t) = (C,\ 1)\left\{\sum_{n=1}^{k} B_n(t)\cdot(1-\cos\overline{N}\pi z)\right\} \tag{19}$$

$$S(z,\ t) = y'(z,\ t) = (C,\ 2)\left\{\sum_{n=1}^{k} B_n(t)\cdot(\overline{N}\pi)\cdot\sin\overline{N}\pi z\right\} \tag{20}$$

$$M(z,\ t) = EIy''(z,\ t) = (C,\ 3)\left\{EI\sum_{n=1}^{k} B_n(t)\cdot(\overline{N}\pi)^2\cdot\cos\overline{N}\pi z\right\} \tag{21}$$

$$V(z,\ t) = EIy'''(z,\ t) = (C,\ 4)\left\{EI\sum_{n=1}^{k} B_n(t)\cdot(\overline{N}\pi)^3\cdot\sin\overline{N}\pi z\right\} \tag{22}$$

$$p(z,\ t) = EIy''''(z,\ t) = (C,\ 5)\left\{EI\sum_{n=1}^{k} B_n(t)\cdot(\overline{N}\pi)^4\cdot\cos\overline{N}\pi\right\} \tag{23}$$

2.3 Determination of B_n Terms

Measured inclinometer data from pile load tests, which implicitly include pile-soil interaction effects, were utilized to determine the coefficients of the derived deflection function by Lin and his colleagues [2,3]. Following similar procedures, the coefficients of $B_n(t)$ are determined from the function of bending moments given in (21), which can be re-written as

$$M(z,\ t) = EIy''(z,\ t) = (C,\ 3)\cdot\left\{EI\sum_{n=1}^{k} B_n(t)\cdot(\overline{N}\pi)^2\cdot\cos\overline{N}\pi z\right\} \tag{24}$$

Since instruments to measure bending moment directly are not available, bending moments are often derived indirectly from curvature and from material properties as follows

$$M = EI\kappa \tag{25}$$

where κ = curvature and is obtained as the difference between compression and tension strains measured at the same depth of the pile shaft divided by the distance between these strain gages. Hence, expanding (24), the computed bending moment at depth z can be presented as (26)

$$[\bar{M}] = [A]\cdot[B] \tag{26}$$

$$\begin{bmatrix} M(z_1)\\ M(z_2)\\ \vdots\\ M(z_j)\end{bmatrix} = \begin{bmatrix} \omega_{n=1}EI\cdot(\overline{N}_{n=1}\pi)^2\cdot\cos\overline{N}_{n=1}\pi z_1 & \omega_{n=2}EI\cdot(\overline{N}_{n=2}\pi)^2\cdot\cos\overline{N}_{n=2}\pi z_1\cdots\omega_{n=k}EI\cdot(\overline{N}_{n=k}\pi)^2\cdot\cos\overline{N}_k\pi z_1\\ \omega_{n=1}EI\cdot(\overline{N}_{n=1}\pi)^2\cdot\cos\overline{N}_{n=1}\pi z_2 & \omega_{n=2}EI\cdot(\overline{N}_{n=2}\pi)^2\cdot\cos\overline{N}_{n=2}\pi z_2\cdots\omega_{n=k}EI\cdot(\overline{N}_{n=k}\pi)^2\cdot\cos\overline{N}_k\pi z_2\\ \vdots & \vdots\\ \omega_{n=1}EI\cdot(\overline{N}_{n=1}\pi)^2\cdot\cos\overline{N}_{n=1}\pi z_j & \omega_{n=2}EI\cdot(\overline{N}_{n=2}\pi)^2\cdot\cos\overline{N}_{n=2}\pi z_j\cdots\omega_{n=k}EI\cdot(\overline{N}_{n=k}\pi)^2\cdot\cos\overline{N}_k\pi z_j\end{bmatrix}\begin{bmatrix} B_1\\ B_2\\ \vdots\\ B_k\end{bmatrix}$$

where

ω_k = Cesàro sum weighting terms

$$[\bar{M}] = \begin{bmatrix} M(z_1)\\ M(z_2)\\ \vdots\\ M(z_j)\end{bmatrix}$$

$$[A] = \begin{bmatrix} \omega_{n=1}EI\cdot(\overline{N}_{n=1}\pi)^2\cdot\cos\overline{N}_{n=1}\pi z_1 & \omega_{n=2}EI\cdot(\overline{N}_{n=2}\pi)^2\cdot\cos\overline{N}_{n=2}\pi z_1\cdots\omega_{n=k}EI\cdot(\overline{N}_{n=k}\pi)^2\cdot\cos\overline{N}_k\pi z_1\\ \omega_{n=1}EI\cdot(\overline{N}_{n=1}\pi)^2\cdot\cos\overline{N}_{n=1}\pi z_2 & \omega_{n=2}EI\cdot(\overline{N}_{n=2}\pi)^2\cdot\cos\overline{N}_{n=2}\pi z_2\cdots\omega_{n=k}EI\cdot(\overline{N}_{n=k}\pi)^2\cdot\cos\overline{N}_k\pi z_2\\ \vdots & \vdots\\ \omega_{n=1}EI\cdot(\overline{N}_{n=1}\pi)^2\cdot\cos\overline{N}_{n=1}\pi z_j & \omega_{n=2}EI\cdot(\overline{N}_{n=2}\pi)^2\cdot\cos\overline{N}_{n=2}\pi z_j\cdots\omega_{n=k}EI\cdot(\overline{N}_{n=k}\pi)^2\cdot\cos\overline{N}_k\pi z_j\end{bmatrix}$$

$$[B] = \begin{bmatrix} B_1\\ B_2\\ \vdots\\ B_k\end{bmatrix}$$

The least-squares rule is then applied to perform regression to solve $[B]$ using procedures described below:

1. Obtain the square summation of the errors, $[S]$, between calculated and measured terms

$$[S] = [B]^T[A]^T[A][B] - 2[B]^T[A]^T[\bar{M}]_m + [\bar{M}]_m^T[\bar{M}]_m \tag{27}$$

where the subscript m represents from measurement.

2. For minimum error, (27) has to be applied and used to solve $[B]$ for $[\bar{M}]_m$ minimized values of coefficients $[B]$

$$\left\{\frac{\partial S}{\partial B}\right\} = 2[A]^T[A][B] - 2[A]^T[\bar{M}]_m = 0 \qquad (28)$$

The bending moments are known at certain discrete locations along the pile so the procedures described above can be adopted to obtain the needed soil resistances and deflections along the pile length at each instant of time.

2.4 Numerical Procedures

(a) Substitute the moment from measured stain gage data into Eq. (27) and then determine $[B]$ from Eq. (28);
(b) Using the deflection function obtained from procedure and utilizing the Cesaro sum technique in Eqs. (21) to (23) to obtain the moment, shear and soil reaction along pile shaft;
(c) Use Eqs. (19) and (23) to generate the *p-y* curves.
(d) Run step (a) to step (c) for different time step to generate the different time step's *p-y* curves.
(f) Use the results of step (d) to plot the *p-y* curve.

3. EXAMPLES

3.1 Brief Description of the Tests

A series of shaking table and push-over tests were conducted at the National Center for Research on Earthquake Engineering (NCREE) in Taiwan. A shear box, invented by Ueng *et al*. [17], was used under one-way cyclic shaking on shaking table. The shear box composes of 15 layers of aluminum alloy inner and outer frames with a specimen size of 1880mm long, 1880mm wide and 1520mm deep. Detailed description regarding the shear box and its functions are in Ueng *et al*. [17]. For push-over tests, a model pile embedded in the same shear box filled with saturated sand was also conducted against the reaction wall at NCREE.

The piles were fabricated from steel pipe with outside diameter of 102mm and a wall thickness of 3mm. In order to measure the pile-soil response to cyclic lateral loading, each pile was instrumented with strain gages at seven different depth throughout the length of the piles (Fig. 1). Lateral cyclic loads were applied at pile head with sine wave type loading for the push-over tests. For shaking table tests, sine waves with frequency of 8Hz and maximum acceleration of 0.03g, were applied at the bottom of the shear box for the duration of 10 seconds. Soil material properties and physical properties of model pile of push-over tests and shaking table tests are listed in Table 1. Summary of the input motion of push-over and shaking table tests is given in Table 2.

3.2 Push-Over Tests

Figure 2 illustrates the set-up of the push-over test. The model piles are embedded 1.32m into the saturated

Table 1 Soil properties and physical properties of model pile

Vietnam sand	D_{10} (mm)	0.19
	D_{50} (mm)	0.3
	Specific gravity, Gs	2.65
	ϕ (°)	35
	Max. void ratio, e_{max}	0.89
	Min. void ratio, e_{min}	0.57
Shear box	Inner length, (cm)	188
	Inner width, (cm)	188
	Outer length, (cm)	234
	Outer width, (cm)	194
	Height, (cm)	152
Model pile	D_o, (cm)	10.2
	D_i, (cm)	9.56
	Thickness, (cm)	0.64
	Length, L (cm)	150
	EI, (kN-m)	226

Table 2 Summary of push-over and shaking table tests

Input motion (Sine Wave)							Soil property
Test	Case	Frequency (Hz)	Amplitude (mm)	Number of cycle	A_{max} (g)	Duration (sec)	D_r (%)
Push-Over test	Case-P1	0.5	2	10	–	–	26*
	Case-P2	2	2	10	–	–	26*
	Case-P3	0.5	5	10	–	–	26*
	Case-P4	2	5	10	–	–	26*
Shaking table test	Case-S1	8	–	–	0.03	10	40*
	Case-S2	8	–	–	0.03	10	82*

* The relative density was measured before test

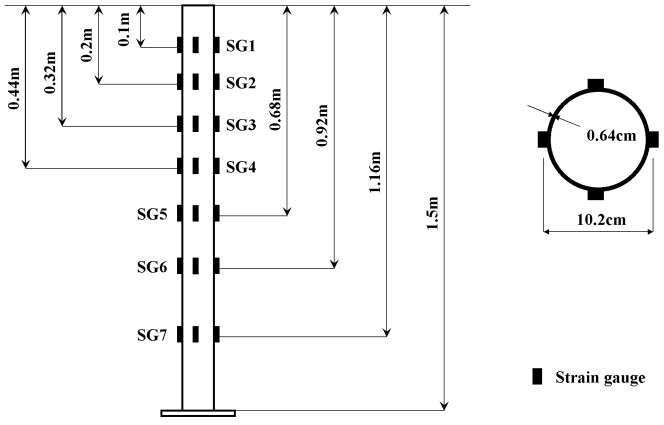

Fig. 1 Instrumented stain gage positions

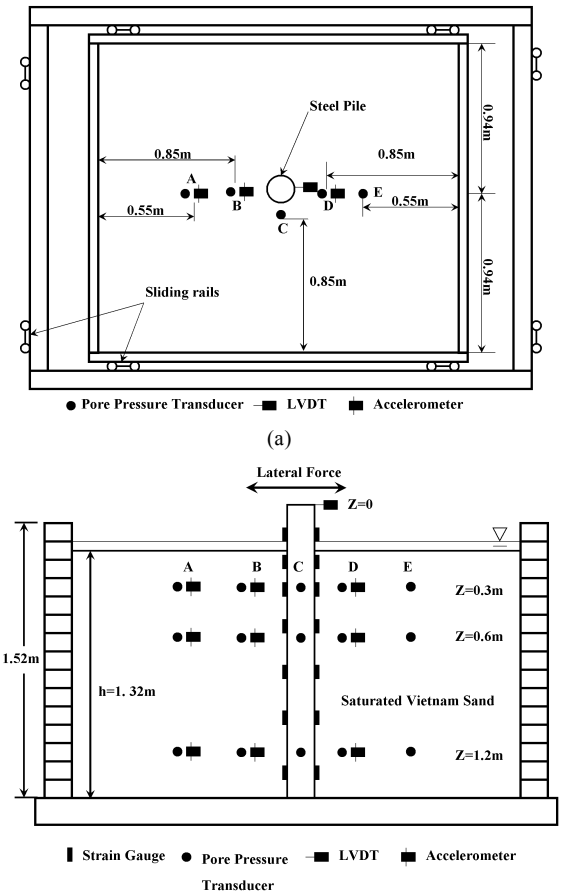

Fig. 2 Test setup of push-over test

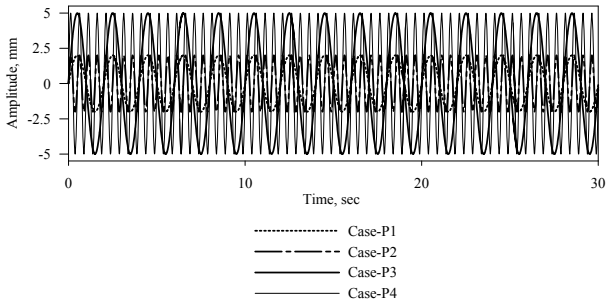

Fig. 3 Input displacement cycles at pile head of the push-over tests

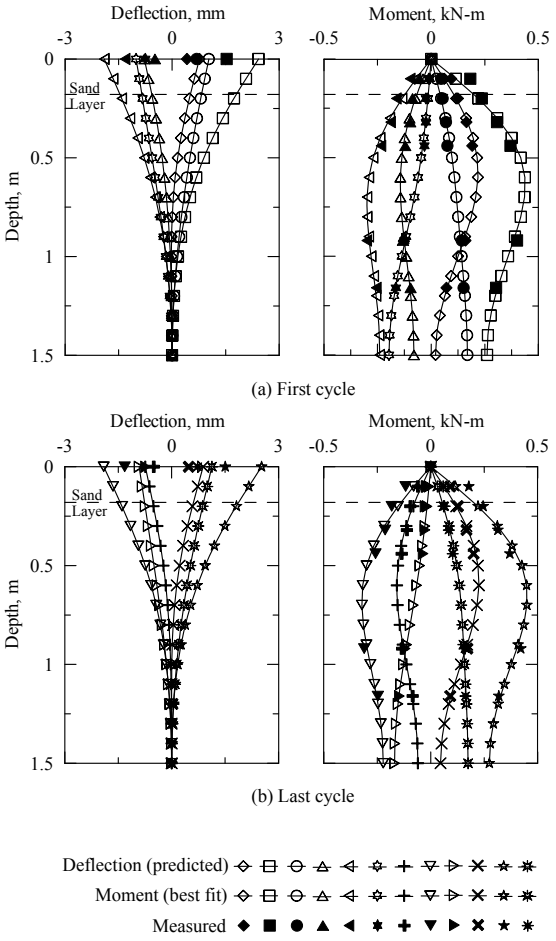

Fig. 4 Pile deflection and bending moment versus depth at various time (Case-P1)

sand layer. Input displacement cycles at pile head are shown in Fig. 3. Derived or measured deflection and moment of the pile versus depth for the first and the last loading cycles of Case-P1 and Case-P2 are given in Figs. 4 and 5, respectively. Under the same loading amplitude, slightly higher pile moment of Case-P2 was observed due to higher input frequency. However, the difference between the deflection of these two tests is small due to small input amplitude. Possibly because of the displacement cycles were applied at 15cm above the pile head via clamping unit, the measured displacement at pile head are smaller than the derived results. The derived dynamic *p-y* curves from test Case-P1 and Case-P2 is shown in Fig. 6, where R_{umax} is the maximum excess pore water pressure ratio and is defined as the ratio of maximum excess pore water pressure vs initial effective confining pressure. The rigidity of derived *p-y* curves increases with depth, and also, the higher the input frequency, the higher the rigidity of the derived *p-y* curves. The hysteretic loop of both tests does not show significant decay because of small input displacement cycles and small numbers of loading cycle.

Excess pore water pressure (PWP) distribution versus depth of Case-P1 and Case-P2 measured at location C of Fig. 2 are shown in Fig. 7, where the R_u is the excess pore water pressure ratio and is defined as the ratio of excess pore water pressure vs initial effective confining pressure. Due to small cyclic loading, the variation of PWP distribution is about identical for each cycle, hence, only the results of the first cycle is shown in the figure. Higher the input amplitude appears to generate higher excess PWP. However, none of the tests has reached the condition of liquefaction.

The derived or measured deflection and moment of the pile for the first and the last loading cycle versus depth of Case-P3 and Case-P4 are shown in Figs. 8 and 9, respectively. Apparently, higher deflection and moment of the pile were observed compared to that of Case-P1 and P2 due to larger loading amplitude. Consequently, the derived *p-y* curves and the measured PWP results are given in Figs. 10 and 11, respectively. Larger hysteretic loop is also found compared to that of

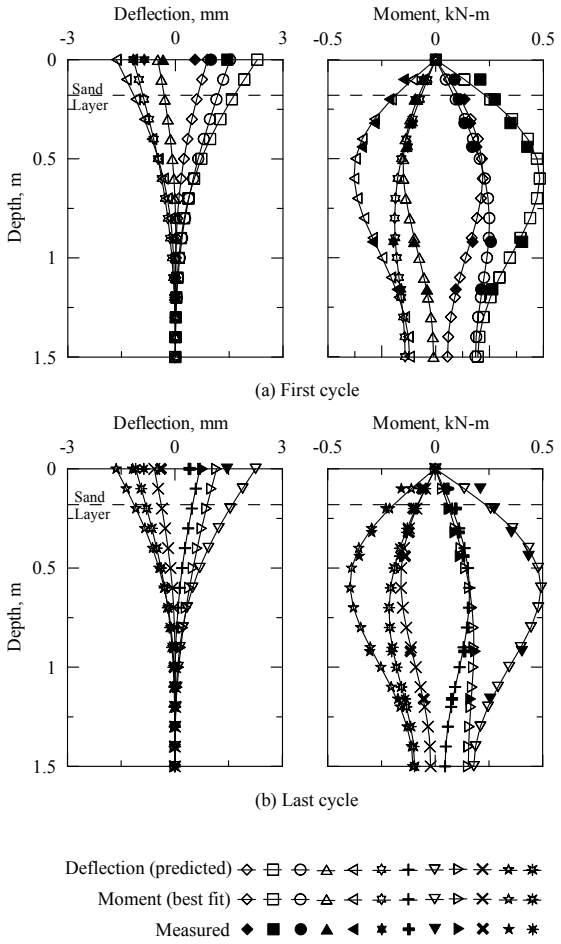

Fig. 5 Pile deflection and bending moment versus depth at various time (Case-P2)

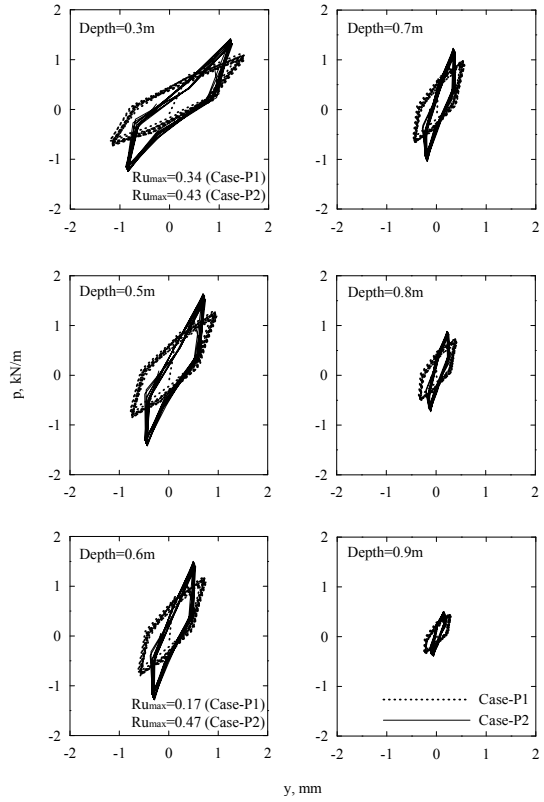

Fig. 6 Derived dynamic *p-y* curves at various depths (Case-P1 and Case-P2)

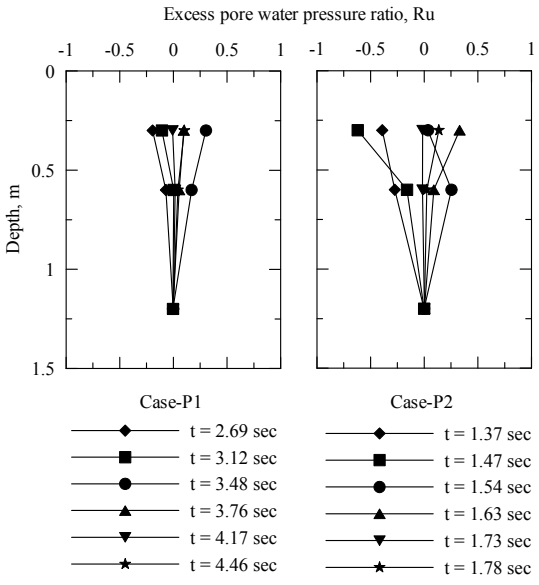

Fig. 7 Measured excess pore water pressure distribution

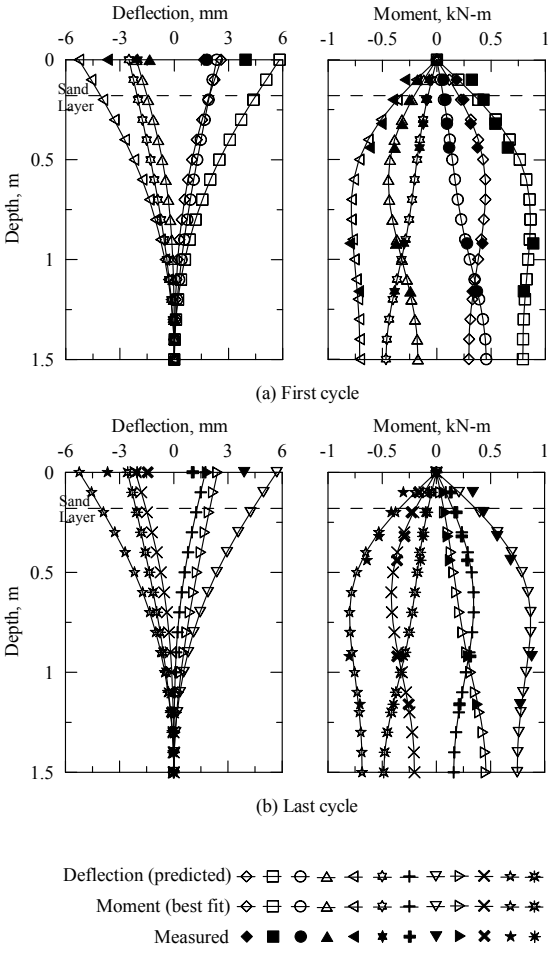

Fig. 8 Pile deflection and bending moment versus depth at various time (Case-P3)

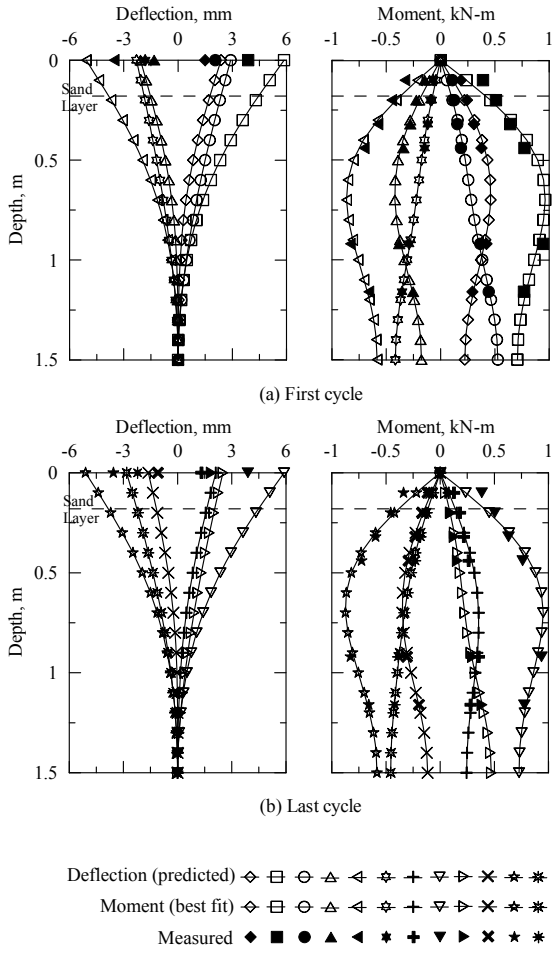

Fig. 9 Pile deflection and bending moment versus depth at various time (Case-P4)

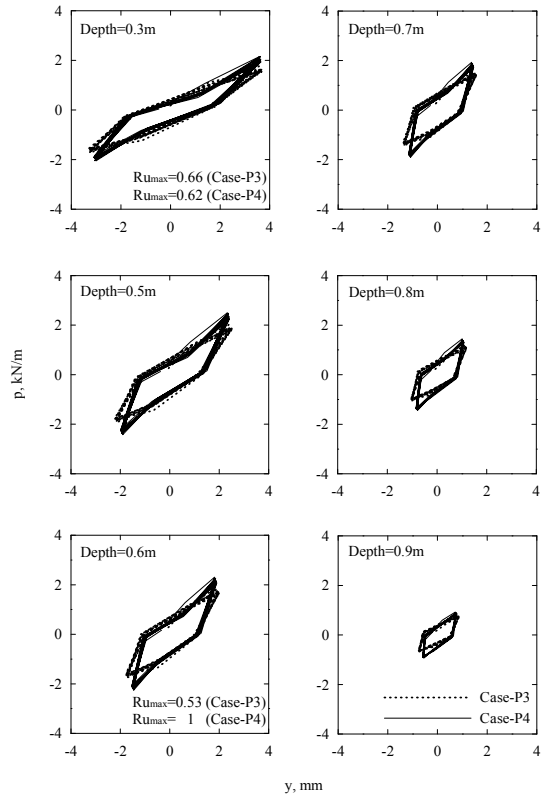

Fig. 10 Derived dynamic *p-y* curves at various depths (Case-P3 and Case-P4)

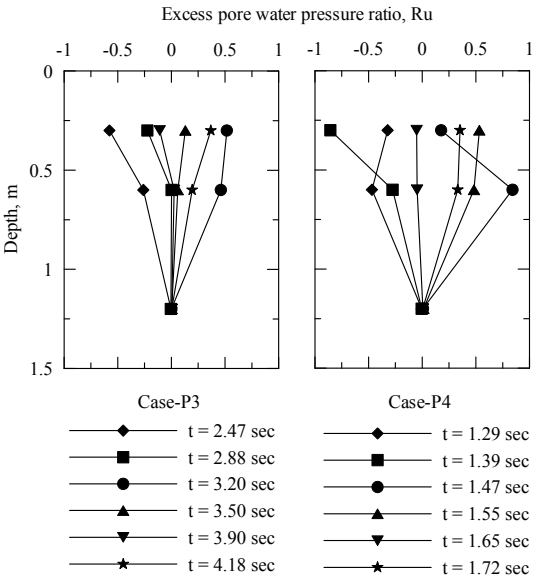

Fig. 11 Excess pore water pressure ratio distribution at various times

Case-P1 and P2. However, the deviation of the rigidity of Case-P3 and P4 is less than that of Case-P1 and P2. In addition, the generated excess PWP of Case-P3 and P4 are higher than that of Case-P1 and P2. The starting point of excess PWP generation is different for each test. Under the same loading frequency, higher amplitude produces higher excess PWP. Again, these tests also do not reach the condition of liquefaction yet.

3.3 Shaking Table Tests

The set-up of the shaking table experiment is illustrated in Fig. 12. Input motion at base of the shear box is given in Fig. 13. Case-S1 and S2 have the same input motion but different soil relative density and different pile embedment as indicated in Table 2. Also, the thickness of the saturated sand layer in the shear box of the Case-S1 and S2 are 1.31m and 1.19m, respectively. The derived or measured deflection and moment along pile shaft of the Case-S1 for the first and last loading cycle is given in Fig. 14. Maximum moment occurs at the tip of the pile due to pile tip boundary condition and because of the loading applied at the base of the shear box. The derived dynamic *p-y* curves at different depths are shown in Fig. 15. The excess PWP at four different measuring locations are given in Fig. 16. At depth of 0.3m below sand layer surface, the condition for liquefaction was observed. Similarly, the deflection/moment versus depth and the derived *p-y* curves for Case-S2 are given in Figs. 17 and 18, respectively. Comparing the difference between Figs. 14 and 17, different soil relative density appears to have quite a different moment and deflection performance, in which Case-S2 shows smaller deflection and smaller moment because of embedded in higher relative density sandy soil and hence has higher confining pressure. Subsequently, under the same shaking condition, the slope of the *p-y* curve of the Case-S1 is higher. Because of higher relative density of Case-S2, excess PWP is almost zero through the entire thickness

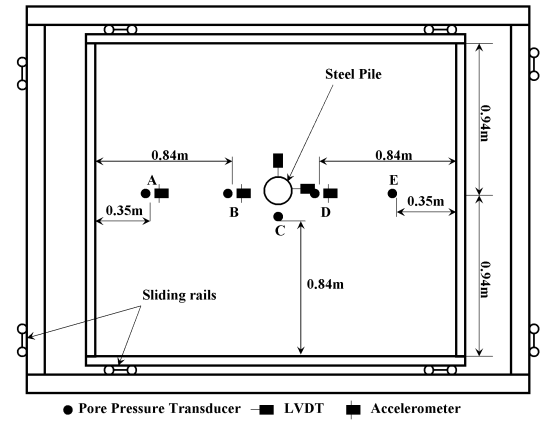

(a)

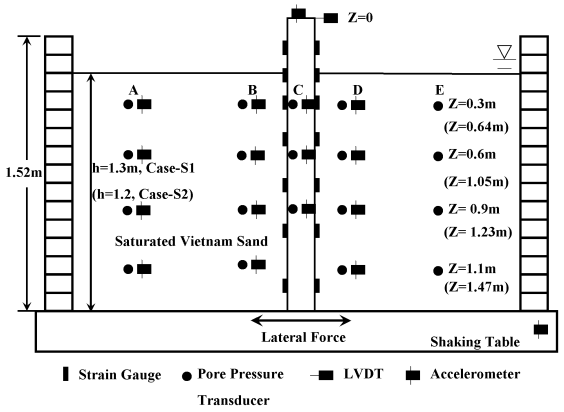

(b)

Fig. 12 Test setup of shaking table test

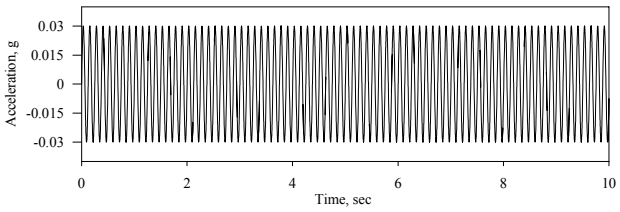

Fig. 13 Input motion at base of the shear box

of the sand layer. Again, the hysteretic loops of Case-S2 are also quite different from those of Case-S1, as shown in Figs. 15 and 18.

Relative to the *p-y* curves obtained from push-over tests, the decay of *p-y* curves obtained shaking table test is more significant. In addition, observing from Fig. 6, Figs. 15 and 18, the slope of the hysteretic loops increases with depth. Also, the area enclosed by the hysteretic loop decreases with depth.

Comparing to the results given in Figs. 15 and 18, the decay of *p-y* curves in the initial certain numbers of loading cycle does not appear too significant because the relative density of sandy soil increases with increasing numbers of loading cycle.

4. SUMMARY AND CONCLUSIONS

In this paper, a relatively simple method was used for interpreting *p-y* curves from instrumented push-over

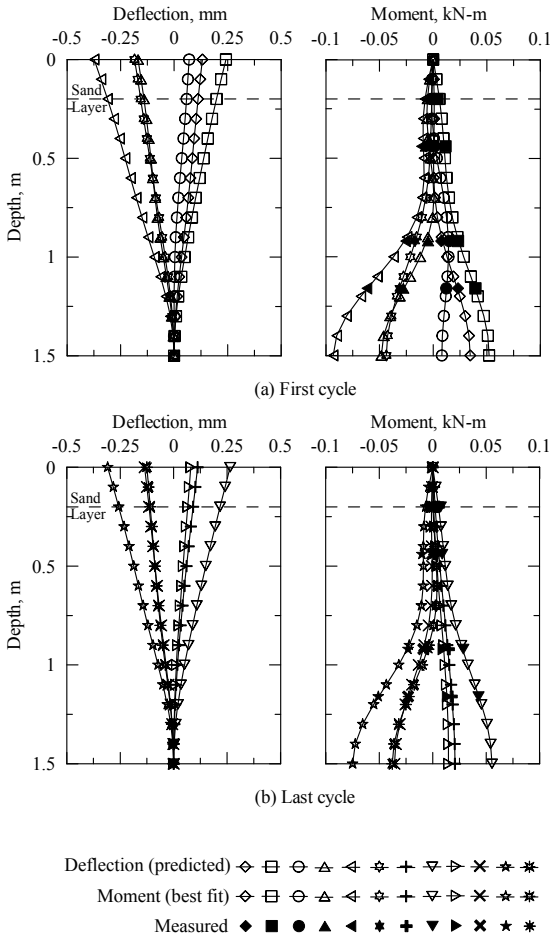

Fig. 14 Pile deflection and bending moment versus depth at various time (Case-S1)

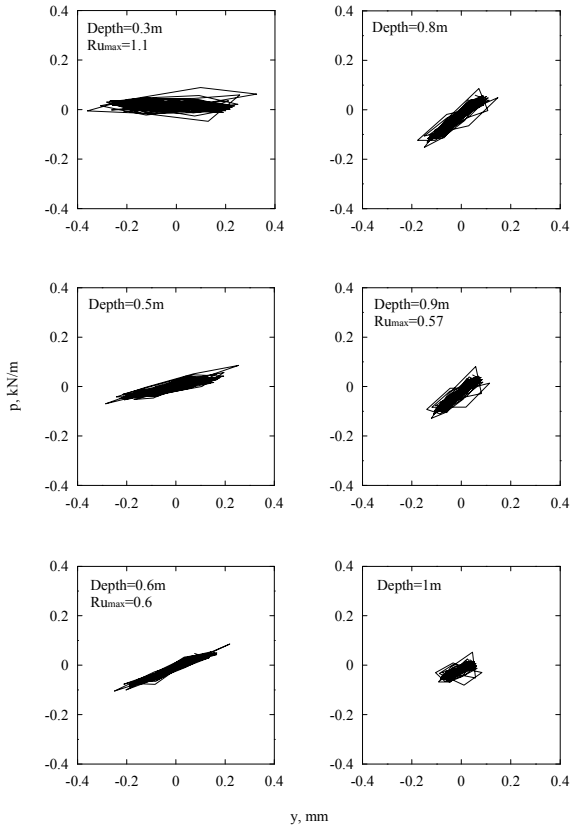

Fig. 15 Derived dynamic *p-y* curves at various depths (Case-S1)

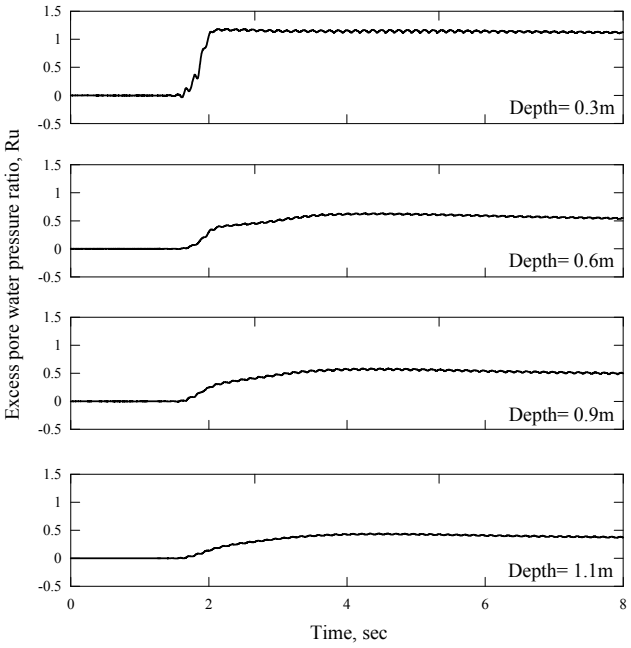

Fig. 16 Excess pore water pressure ratio at different depths of Case-S1 test

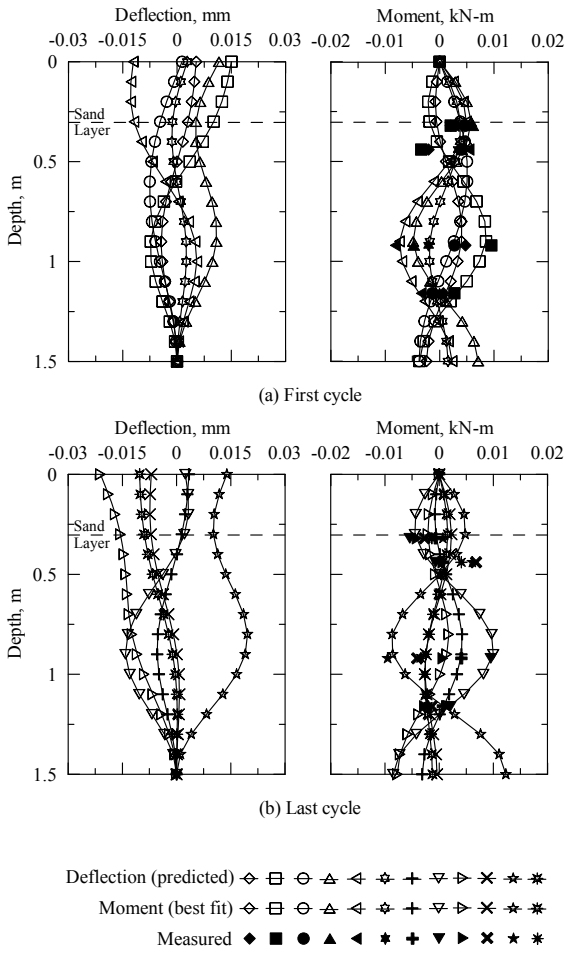

Fig. 17 Pile deflection and bending moment versus depth at various time (Case-S2)

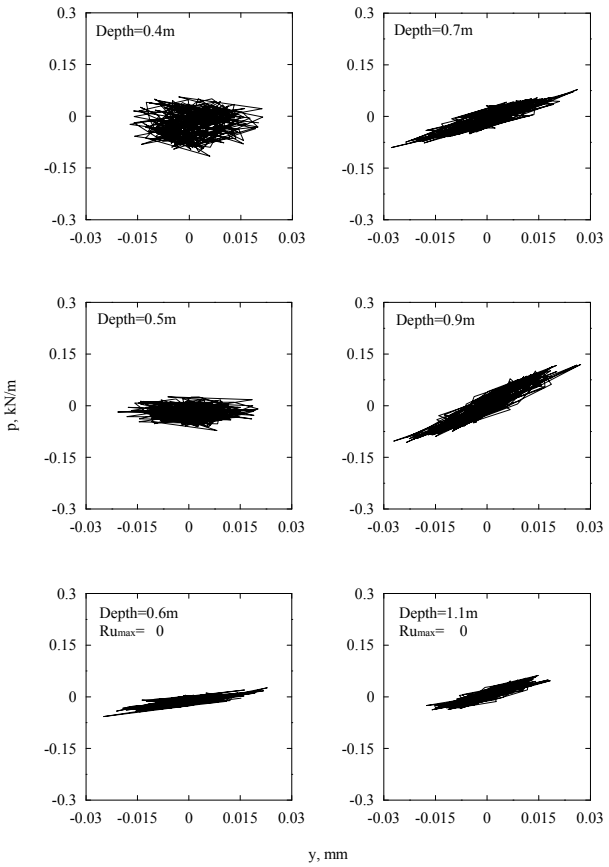

Fig. 18 Derived dynamic *p-y* curves at various depths (Case-S2)

and shaking table pile test results. Background theories, as well as detailed derivation of the proposed analytical method were described in this paper. Moreover, the feasibility of the developed method was further verified using results of six real case histories. Advantages of the proposed analytical method include (1) only either inclinometer data or strain gage data is needed for deriving the deflection or the curvature function, respectively; (2) the derived deflection or curvature function can be used to describe lateral behaviors of a single pile system, such as *p-y* curves, satisfying various boundary conditions of the pile.

Some observations were found from the studied push-over and shaking table tests. For push-over tests: (a) Under the same loading amplitude, slightly higher pile moment of Case-P2 was observed due to higher input frequency; (b) The rigidity of derived *p-y* curves increases with depth, and also, the higher the input frequency, the higher the rigidity of the derived *p-y* curves; (c) The hysteretic loop of both tests does not show significant decay because of small input displacement cycles and small numbers of loading cycle. For shaking table tests: (a) Case-S2 shows smaller deflection and smaller moment because of embedded in higher relative density sandy soil and hence has higher confining pressure; (b) Relative to the *p-y* curves obtained from push-over tests, the decay of *p-y* curves obtained shaking table test is more significant; (c) observing from Figs. 6, 15 and 18, the slope of the hysteretic loops increases with depth. Also, the area enclosed by the hysteretic loop decreases with depth.

For short piles with high lateral loading, permanent lateral displacement might occur at bottom of piles. Definitions of strain energy and potential energy used in this study need to be modified in order to establish the energy conservation relation for this case. Further study is needed to develop analytical model for short pile applications.

ACKNOWLEDGEMENTS

The research described in this paper was sponsored by the National Science Council under grant number NSC 96-2221-E-019-025-MY2 and by the National Center for Research on Earthquake Engineering (NCREE) in Taiwan. Their support is deeply appreciated.

REFERENCES

1. Liao, J. C. and Lin, S. S., "An Analytical Model for Deflection of Laterally Loaded Piles," *Journal of Marine Science and Technology*, **11**, pp. 149–154 (2003).
2. Lin, S. S. and Liao, J. C., "Lateral Response Evaluation of Single Piles Using Inclinometer Data," *Journal of Geotechnical and Geoenvironmental Engineering,* **132**, pp. 1566–1573 (2006).
3. Lin, S. S., Liao, J. C., Chen, J. T. and Chen, L., "Lateral Performance of Piles Evaluated via Inclinometer Data," *Computers and Geotechnics,* **32**, pp. 411–421 (2005).
4. Yang, K. and Liang, R., "Methods for Deriving P-Y Curves from Instrumented Lateral Load Tests," *Geotechnical Testing Journal,* **30**, pp. 31–38 (2007).
5. Reese, L. C. and Welch, R. C., "Lateral Loading of Deep Foundations in Stiff Clay," *Journal of Geotechnical Engineering*, ASCE, **101**, pp. 633–649 (1975).
6. Matlock, H. and Ripperger, E. A., "Procedures and Instrumentation for Tests on a Laterally Loaded Pile," *Proceedings 8th Texas Conference on Soil Mechanics and Foundation Engineering*, Austin, Texas (1956).
7. Dou, H. and Byrne, P. M., "Dynamic Response of Single Piles and Soil-Pile Interaction," *Canadian Geotechnical Journal,* **33**, pp. 80–96 (1996).
8. Shirato, M., Koseki, J., Fukui, J. and Kimura, Y., "Effects of Stress-Dilatancy Behavior of Soil on Load Transfer Hysteresis in Soil-Pile Interaction," *Soils and Foundations*, **46**, pp. 281–298 (2006).
9. Wilson, D., "Soil-Pile-Superstructure Interaction in Liquefying Sand and Soft Clay," Ph.D. Dissertation, University of California at Davis (1998).
10. Sousa Coutinho, A. G. F., "Data Reduction of Horizontal Load Full-Scale Tests on Bored Concrete Piles and Pile Groups," *Journal of Geotechnical and Geoenvironmental Engineering*, ASCE, **132**, pp. 752–769 (2006).
11. Dyson, G. J. and Randolph, M. F., "Monotonic Lateral Loading of Piles in calcareous Sand," *Journal of Geotechnical and Geoenvironmental Engineering*, **127**, pp. 346–352 (2001).
12. Ooi, P. S. K. and Ramsey, T. L., "Curvature and Bending Moments from Inclinometer Data," *International Journal of Geomechanics*, **3**, pp. 64–74 (2003).
13. Brown, D. A., Reese, L. C. and O'Neill, M. W., "Behavior of a Large Scale Pile Group Subjected to Cyclic Lateral Loading," *Journal of Geotechnical Engineering,* ASCE, **113**, pp. 1326–1343 (1987).
14. Pinto, P. L., Anderson, B. and Townsend, F. C., "Comparison of Horizontal Load Transfer Curves for Laterally Loaded Piles from Strain Gages and Slope Inclinometer: A Case Study," *Field Instrumentation for Soil and Rock,* ASTM STP 1358, pp. 3–15 (1999).
15. Hardy, G. H., *Divergent Series*, Oxford Univ. Press, London (1949).
16. Ueng, T. S., *Research Repot of Biaxial Shear Box at NCREE on Year 2008*, National Center for Research on Earthquake Engineering (2008).
17. Ueng, T. S., Wang, M. H., Chen, M. H., Chen, C. H., and Peng, L. H., "A Large Biaxial Shear Box for Shaking Table Test on Saturated Sand," *Geotechnical Testing Journal*, **29**, pp. 1–8 (2006).

(Manuscript received February 2, 2009,
accepted for publication June 10, 2009.)